Chapter 4

Wasp - Waisted loop and Spin frustration in $Dy_{2-x}Eu_xTi_2O_7$ Pyrochlore

4.1 Introduction:

Physical systems with interacting degrees of freedom are excellent playground to study the geometrical frustration as they possess competing magnetic interactions. These competing interactions drive the systems into macroscopically degenerate numerous ground states at low temperature [195-197]. The exotic magnetic ground states can be classified as classical dipolar spin ice [53, 160], quantum spin ice [198], spin slush [199], quantum spin liquid states [200, 201], spin glass [170] and order by disorder states [204-205] etc. Apart from the balancing dipolar interactions, exchange interactions and strong crystal fields also contribute in generating these novel and riveting ground states. Pyrochlore structure (space group Fd-3m) which is a well-known geometrically frustrated system has an empirical formula $A_2^{3+}B_2^{4+}O_7$ or $A_2B_2O_6O'$ in which A-site (16d Wyckoff position) contains rare earth ions and B-site (16c) accommodates transition metal ions. The rare earth cation A^{3+} is surrounded by eight oxygen anions [six O (48f) ions and two O′ (8b) ions] whereas transition metal cation B^{4+} is coordinated with six oxygen anion O (48f) in $A_2^{3+}B_2^{4+}O_7$ structure. Therefore, ordered pyrochlore structure is defined as an arrangement of two interpenetrating networks of BO_6 octahedral and A_2O' chains and thus, it is constituted of a three-dimensional array of corner sharing tetrahedra [182]. Among all the frustrated systems, the spin ice state has its own forte, as in these materials, ferromagnetic interactions, dipole exchange interactions, strong single-ion Ising anisotropy and crystal field effects contrive the spins of rare earth ions to align directly towards (two spins) and away (two spins) from the centre of the tetrahedral [206-212]. This “two-in/two-out” arrangement of spins is similar to the arrangement of hydrogen ions in water ice [12]. Although, theoretical calculations suggest a long range ordered state [213] to possess non zero-point entropy for these spin ice materials, experimentally, they do

not show any signature of long range ordering in zero magnetic field. The spins freeze into a non-equilibrium low temperature state around same zero point entropy as water ice [59]. Recently, it has been observed that the existence of coulomb phase with dipolar interaction in spin ice materials elevate to magnetic monopole [214-216].

$Dy_2Ti_2O_7$ (DTO) is an acclaimed spin ice pyrochlore system in which Dy^{3+} ions (having 7f e^- with J = 15/2) reside on a lattice of corner sharing tetrahedra. The uniaxial anisotropy of these Dy^{3+} ions which points along <111> axis causes the Ising type ground state doublet with a large gap of ~ 200 K below the first excited state [11, 208]. The reported Curie-Weiss temperature (θ_{CW}) of DTO pyrochlore is ~1 K [53]. It has been reported from the specific heat measurement of DTO compound that spin freezes out only below the T_i = 4 K [210]. However, AC susceptibility study shows two novel dynamic spin freezing at T_i ~ 4 K and T_f ~ 16 K. The low temperature transition at T_i ~ 4 K is associated to entering the spin ice manifold [159, 217] and the high temperature spin dynamics (at T_f ~ 16 K) has been attributed to spin flip process [54, 218]. This spin relaxation mechanism of DTO shows a surprising classical to quantum double cross over upon cooling. At, T_f ~ 16 K DTO shows thermally activated relaxation phenomenon and at T_{cross} ~13 K, the mechanism changes to quantum tunneling. Further, at T_i ~ 4 K, it reverts back to thermally activated relaxation from quantum tunneling. Development of spin correlations is thought to be the reason behind the cross over [56]. Eventually, the presence of high temperature spin freezing (T_f~ 16 K) makes DTO system more fascinating among all spin ice systems as other spin ice compounds do not show such high temperature spin freezing. Moreover, $Dy_2Ti_2O_7$ is renowned not only for magnetic properties but also for its electric conductivity [219], dielectric and magneto dielectric responses [220, 221]. Another frustrated pyrochlore system $Eu_2Ti_2O_7$ (ETO) exhibits

antiferromagnetic interaction as it has negative Curie-Weiss temperature (~ θ_{CW} = - 1.35 K) [67]. Moreover, $Eu_2Ti_2O_7$ possesses an XY planar antiferromagnetic pyrochlore lattice structure which does not order down to 1.8 K. Although, ETO has a non magnetic ground state, it shows substantial magnetic moment and strong crystal field effect which generates single ion anisotropy parallel to <111> axis [66]. An exotic spin freezing transition around T_s = 35 K was found in AC susceptibility study of ETO compound, which is highest reported spin freezing transition so far in geometrically frustrated pryrochlore systems [67].

In recent years, there have been substantial efforts in studying both (A and B) sites doped $Dy_2Ti_2O_7$ which show modification in the spins arrangement and alter the low temperature magnetic states [222-223]. Snyder et al have shown that substitution of Dy^{3+} ions by non-magnetic (Y^{3+} or Lu^{3+}) ions causes the reemergence of high temperature spin freezing transition which shifts towards higher temperature with increasing doping concentration [218]. Not only non-magnetic diluents [218] but also magnetic elements (like Tb^{3+} ion) show drastic change in the ground state of $Dy_xTb_{2-x}Ti_2O_7$ pyrochlore [194]. In this context, it would be interesting to study the magnetic interaction and spin relaxation mechanism when Dy^{3+} ions are replaced by Eu^{3+} ions in DTO spin ice compound as both the compounds (DTO and ETO) show spin freezing around 16 K and 35 K respectively. Additionally, the low temperature magnetic property changes with the increasing Eu (x) content in $Dy_{2-x}Eu_xTi_2O_7$, as the crystal field is expected to evolve very strongly from an ising system along the local z-axis to a planar XY antiferromagnetic system. In the present investigation, we have carried out extensive analysis of $Dy_{2-x}Eu_xTi_2O_7$ (DETO) ($0 \leq x \leq 2.0$) through structural, Raman, DC and AC susceptibility measurements.

4.2 Experimental detail:

$Dy_{2-x}Eu_xTi_2O_7$ ($0 \leq x \leq 2.0$) polycrystalline samples were prepared by conventional solid state reaction method. High purity (99.999%) starting materials for the synthesis were Dy_2O_3, Eu_2O_3 and TiO_2. Same synthesis process was followed to synthesize the present series of samples as reported elsewhere [224]. All DETO samples were confirmed to be single phase pyrochlore without any chemical impurity from powder X-ray diffraction (XRD) at room temperature. XRD patterns of samples were recorded in Rigaku Miniflex II X-ray diffractometer using Cu Kα radiation. The DC and AC magnetic measurements of each sample were performed using a Quantum Design magnetic property measurement system (MPMS) super conducting quantum interference device (SQUID) magnetometer. Raman spectroscopic measurements were carried out at room temperature, using Renishaw Micro Raman Spectrometer with a solid state laser of wavelength 532 nm.

4.3 Results and Discussions:

4.3.1 Stability and Structural Analysis:

The ionic radius ratio of A^{3+} and Ti^{4+} cations is the key factor to determine the stability of $A_2Ti_2O_7$ pyrochlore. For pyrochlore structure, value of $r(A^{3+})/r(Ti^{4+})$ (R) lies between 1.46 - 1.78 where r stands for the radius of the respective element. For R< 1.46, the structure becomes a defect fluorite and a perovskite layered structure forms for R>1.78 [182]. We have calculated the stability determining factor of DETO samples using the following equation [183]

$$\frac{r(A^{3+})}{r(Ti^{4+})} = \frac{(1-x)r(Dy^{3+}) + xr(Eu^{3+})}{r(Ti^{4+})} \quad (4.1)$$

Shannon ionic radii of Dy^{3+}, Eu^{3+}, Ti^{4+} ions (1.027 Å, 1.066 Å, 0.605 Å respectively) were used to estimate the stability factor. The obtained ionic radius ratio using eq. (4.1) are shown in Table 4.1 which shows that the stability factors of all the compounds are in the range of pyrochlore structure. As the Eu content enriches in DETO samples, the $r(A^{3+})/r(Ti^{4+})$ ratio increases linearly which reflects the enhancement of disorderness in the structure.

Sample	**x = 0.0**	**x = 0.5**	**x = 1.0**	**x = 1.5**	**x = 1.8**	**x= 1.9**	**x = 2.0**
$r(R^{3+})/r(Ti^{4+})$	1.69	1.714	1.73	1.75	1.755	1.758	1.762

Table 4.1: The ionic radius ratio of DETO series compounds.

The room temperature X-ray diffraction pattern of each DETO sample confirms single phase face centered cubic pyrochlore structure with space group Fd-3m [inset (i) of figure 4.1]. The phase purity, homogeneity and unit cell dimension of all the samples were verified by Rietveld analysis of XRD data using FULLPROF program [184].

Inset (ii) of figure 4.1 shows the XRD pattern Rietveld refinement of $Dy_{1.0}Eu_{1.0}Ti_2O_7$. Evaluated lattice parameters of (x=0 and x=2.0) samples are in good agreement with earlier reports [224, 225]. The variation of lattice constant with Eu concentration is shown in figure 4.1. The graph shows that the value of lattice constant increase linearly with Eu concentration obeying the Vegard's law except slight deviation at x=1.9 (figure 4.1). Dy (Eu)-Ti antisite disorder might cause such deviation from Vegard's law for x = 1.9.

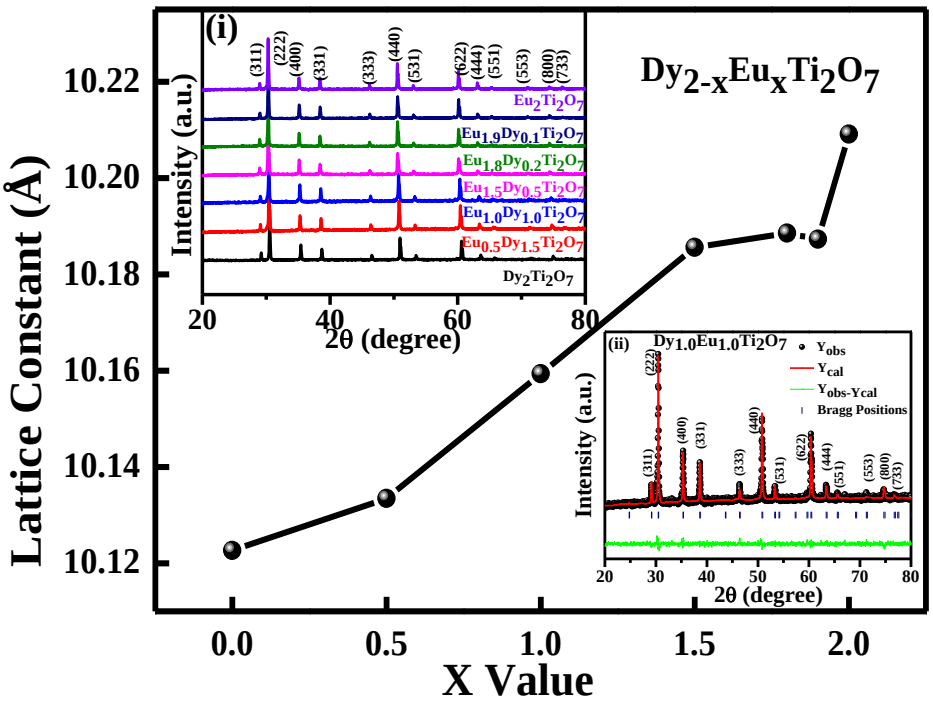

Figure 4.1: The lattice constant (Cubic Structure) of $Dy_{2-x}Eu_xTi_2O_7$ as a function of x value. Inset **(i):** X-ray powder diffraction pattern for the $Dy_{2-x}Eu_xTi_2O_7$ samples. Inset **(ii):** Rietveld refinement for the $Dy_{1.0}Eu_{1.0}Ti_2O_7$ sample

4.3.2 Raman Spectroscopy Analysis:

Figure 4.2 shows the Raman spectra of DETO samples in the wave number range of 100 – 1000 cm^{-1}. Factor group analysis suggested that for a geometrically frustrated pyrochlore structure, there exist total six Raman active modes ($A_{1g}+E_g+4F_{2g}$) and seven infrared active modes ($7F_{1u}$) [189]. Based on earlier reports, we have labeled all six Raman modes in figure 4.2 [226]. The most intense peak at ~ 305 cm^{-1} contains two Raman modes ($F_{2g}+ E_g$) in which F_{2g} and E_g modes are due to O-Dy(Eu)-O bending and O- sublattice vibration respectively. The second intense peak at ~ 518 cm^{-1} (A_{1g}) mode is related to the stretching of Dy (Eu)-O bond. The lowest frequency band near 215 cm^{-1} is assigned to F_{2g} mode which is

associated to O′sublattice vibration. The rest two F_{2g} Raman modes are located at ~ 445 cm^{-1} and ~ 581 cm^{-1} respectively [227]. The peak at ~ 682 cm^{-1} (denoted by *) is not assigned to as forbidden IR mode because DETO samples are less defective pyrochlore. Thus, this band can be attributed to second order excitations [191].

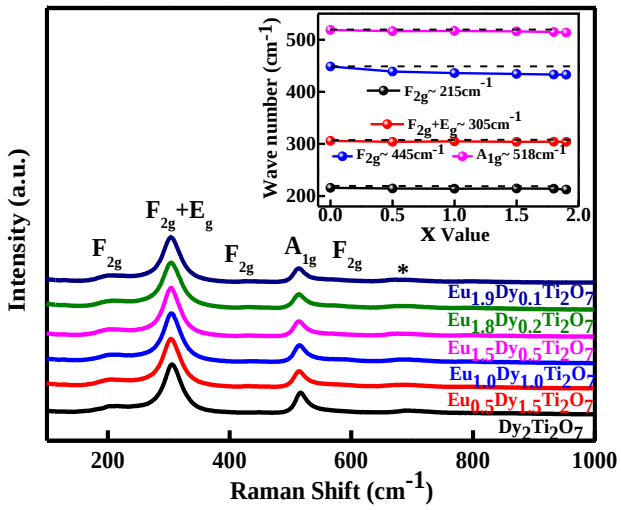

Figure 4.2: Raman spectra of the $Dy_{2-x}Eu_xTi_2O_7$ samples at 300 K. **Inset**: Variation of four active phonon modes as a function of x in $Dy_{2-x}Eu_xTi_2O_7$ samples along with the straight horizontal dashed lines for reference.

Inset of figure 4.2 shows the variation of four phonon energies (wavenumber of the Raman modes) with Eu content (x) in $Dy_{2-x}Eu_xTi_2O_7$. From the figure, it is clear that all the four modes (F_{2g} ~ 215cm^{-1}, F_{2g}+E_g ~ 305cm^{-1}, F_{2g} ~ 445cm^{-1}, A_{1g} ~ 518cm^{-1}) show red shift i.e. softening of the modes with increasing Eu content. The location of Raman active modes depends on the band strength (bond length) and ionic mass. In DETO samples, lattice constant increases with increasing Eu content resulting in the shift of phonon modes to lower frequencies. Interestingly, all four phonon modes shift towards lower frequencies for all the DETO samples as shown in inset of figure 4.2. Although, a violation has been found in lattice constant variation for $Dy_{0.1}Eu_{1.9}Ti_2O_7$ (x = 1.9) from XRD data, the systematic red

shift in all phonon modes with increasing Eu concentration in $Dy_{2-x}Eu_xTi_2O_7$ confirms that Dy^{3+} ions are substituted by Eu^{3+} ions.

4.3.3 Magnetization Analysis:

4.3.3.1 DC magnetic Study:

The DC susceptibility for DETO system at ZFC protocol is shown in figure 4.3a. DTO compound has the largest magnetic moment among all the studied samples. The DC magnetization value decreases drastically with substitution of Eu^{3+} ion at Dy^{3+} site. Decay in magnetization value in Eu doped samples can be attributed to lower magnetic moment Eu^{3+} (3.46 μ_B) than Dy^{3+} (10.62 μ_B). Exchange interactions between Eu-Dy and Eu-Eu spins are also responsible for the decrease in magnetization. $\chi(T)$ curves for x = 0, 0.50, 1.0 (figure 4.3a) follow the standard Curie-Weiss (CW) law [$\chi = C/(T - \theta_{CW})$, where C is Curie-constant and θ_{CW} is Curie-Weiss temperature] in whole temperature range (2-300 K) of measurement. However, the low temperature magnetization data for x = 1.5, 1.8, 1.9 do not follow the standard CW law as shown in inset (i) of figure 4.3a. For ETO compound, the $\chi(T)$ data could not be fitted with CW law due to the presence of strong plateau region (20-90 K) as shown in inset (ii) of figure 4.3a. The plateau region is attributed to crystal-field effect [66]. The inverse DC magnetic susceptibility ($1/\chi$) vs. temperature (T) plots of all DETO samples are shown in figure 4.3b. Linear curves are found for x = 0, 0.50, 1.0 samples as they follow CW law in whole temperature range whereas a sharp down turn is found for x = 1.5, 1.8, 1.9, 2.0 samples at lower temperature. This unusual nature of $\chi^{-1}(T)$ for x = 1.5, 1.8, 1.9, 2.0 suggests presence of other interactions viz. exchange interactions, dipolar exchange interactions etc, along with crystal-field interactions [192].

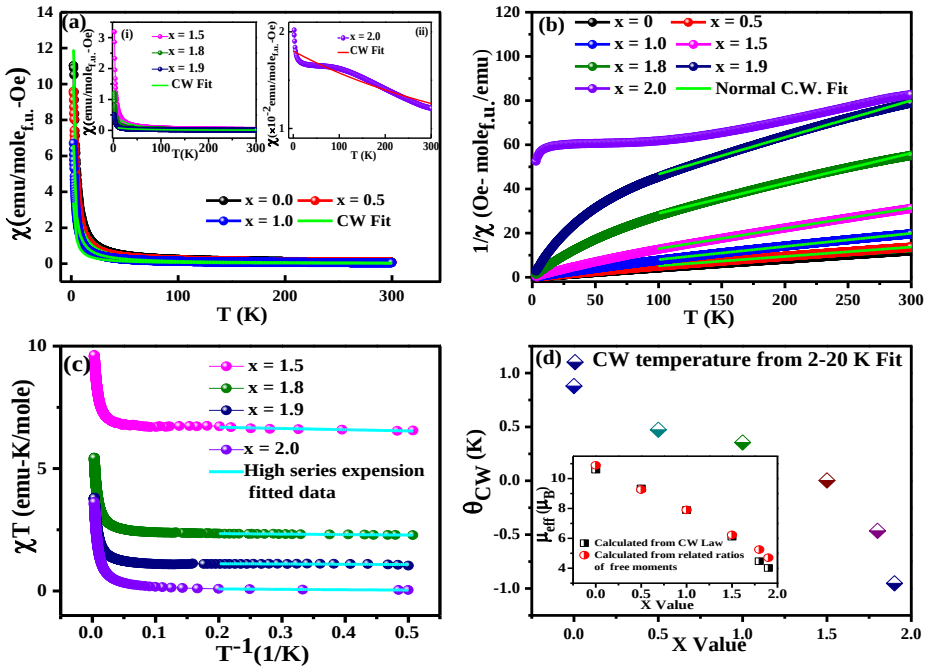

Figure 4.3(a): The temperature dependent DC magnetic susceptibility (ZFC) with standard Curie-Weiss fit of the x = 0.0, 0.5, 1.0 samples. Inset **(i):** The temperature dependent DC magnetic susceptibility (ZFC) with standard Curie-Weiss fit of the x = 1.5, 1.8, 1.9 samples. Inset **(ii):** χ vs. T curve of x = 2.0 sample with standard CW fit. **(b):** Inverse DC susceptibility vs. T curve of $Dy_{2-x}Eu_xTi_2O_7$ compounds with inverse CW fit at (100-300 K). **(c):** High temperature series expansion fit for $Dy_{2-x}Eu_xTi_2O_7$ (x = 1.5, 1.8, 1.9, 2.0) samples. **(d):** Variation of derived CW temperature with x value of $Dy_{2-x}Eu_xTi_2O_7$ series from (2-20 K) CW fit. Inset: Variation of calculated effective magnetic moments with Eu content (x) derived from inverse CW fit at high temperature (100-300 K) for DETO samples.

To estimate the contribution of these magnetic interactions (viz. exchange interactions, dipolar exchange interactions), we have fitted the susceptibility data with the following equation [66];

$$\chi = C\left[\left(\frac{1}{T}\right) + \left(\frac{\theta_{Cw}}{T^2}\right)\right] \tag{4.2}$$

The graph between χT vs. $1/T$ is displayed in figure 4.3c. The values of θ_{CW}, effective magnetic moment (μ_{eff}), exchange interaction energy (J_{nn}) and dipolar interaction energy (D_{nn}) were extracted from linear fit on χT vs. $1/T$ data for (2-5 K) temperature range. D_{nn} values are obtained from $D_{nn} = \frac{\mu_0 \mu_{eff}^2}{4\pi r_{nn}^3}$ where, 'a' is the lattice constant of the unit cell of the

system and r_{nn} is the distance between a A^{3+} ion at (*0, 0, 0*) and its nearest neighbour at (*a/4, a/4, 0*). Only classical interactions are considered here, therefore, classical exchange interaction energy (J^{cl}) was determined by the formula, $J^{cl}= S(S+1)J_{nn}$ and $J_{nn} = 3\theta_{CW}/zS(S+1)$ [here $z = 6$ is the co-ordination number][66]. The experimental effective magnetic moment was calculated by using formula, $C = \frac{N\mu_{eff}^2}{3k}$ where, *N* is Avogadro's number and *k* is Boltzmann constant. All the obtained values are shown in Table 4.2. The change of sign of the θ_{CW} going from a spin ice type system (DTO) to an antiferromagnetic system (ETO) also suggests that the exchange interactions will be profoundly modified, while the dipolar interaction (D_{nn}) will smoothly decrease because of lattice parameter increase. Moreover, this nature for x = 1.5, 1.8, 1.9, 2.0 samples confirm the increase of antiferromagnetic interactions.

Sample	θ_{CW} **(K)**	J^{cl} **(K)**	D_{nn} **(K)**	μ_{eff} (μ_B)
$Dy_{0.5}Eu_{1.5}Ti_2O_7$	-0.074	-0.037	0.3615	5.21
$Dy_{0.2}Eu_{1.8}Ti_2O_7$	-0.0826	-0.0413	0.1260	3.088
$Dy_{0.1}Eu_{1.9}Ti_2O_7$	-0.099	-0.0496	0.06037	2.13
$Eu_2Ti_2O_7$	-1.35	-0.6742	0.00609	0.679

Table 4.2: Extracted Curie–Weiss temperature, classical exchange energy, dipolar interaction energy and calculated magnetic moment of (x = 1.5, 1.8, 1.9, 2.0) samples by high temperature series expansion fit [2-5 K].

We have also extracted the μ_{eff} values of $Dy_{2-x}Eu_xTi_2O_7$ samples from inverse CW law fit (inverse CW law fit is shown in fig. 4.3b) at high temperature range (100-300 K). As the magnetic moment of both Dy and Eu ions are responsible for total magnetization value, the

high temperature theoretical paramagnetic moment of all the samples are calculated using the equation, $\mu^2_{eff} = x\mu^2_{Dy} + y\mu^2_{Eu}$ to compare it with the experimental one. Here, *x* and *y* are number of Dy and Eu atoms per f.u. of $Dy_{2-x}Eu_xTi_2O_7$ respectively and μ_{Dy} and μ_{Eu} are the effective magnetic moment of Dy and Eu ions respectively. Variation of effective magnetic moments (both theoretical and experimental) with x is shown in inset of figure 4.3d. The experimental magnetic moment values are comparable to that of theoretically obtained for x = 0, 0.50, 1.0, 1.5 samples. However, for x = 1.8, 1.9 samples, the theoretical value of μ_{eff} /Dy (Eu) is larger than that of the experimental which suggests the strong magnetic correlations between Dy and Eu spins in those samples.

The values obtained from CW fit are reported to be very sensitive to selected temperature range [228]. In the present case, CW fit also described the data well in 2-20 K temperature range which is also appropriate for the lowest crystal-field excitations. From the inverse linear CW fit at low temperature, we have derived the θ_{CW} values for all samples which are shown in figure 4.3d. The obtained values of θ_{CW} are significantly positive for x = 0, 0.50, 1.0 samples, whereas for x = 1.5, 1.8, 1.9, 2.0, it becomes negative.

The magnetic field dependent magnetization (*M-H)* curves of $Dy_{2-x}Eu_xTi_2O_7$ at 2 K are shown in the inset of figure 4.4a. All the curves get saturated with nearly same saturation magnetization value [M_s = 5 μ_B/Dy]. The parent DTO compound is also saturated at ~5 μ_B/Dy, which is almost half of its theoretical value. Single ion anisotropy and powder averaging effect cause the magnetic moment of DTO to saturate at ~ 5 μ_B/Dy. Similar behaviour is observed for all doped samples. Saturation in magnetization around half of its theoretical value suggested that Dy spins induce Ising anisotropy. As shown in figure 4.4a,

interesting *M-H* behaviour is observed for x = 1.5, 1.8, 1.9 samples. For these samples, the coercivity becomes minimum i.e., magnetization value at very low magnetic field becomes low. However, a loop is observed at high magnetic field. Such hysteresis loop is typically known as wasp-waisted hysteresis (WWH) loop [229, 230]. Similar M-H loops are commonly observed in mixed magnetic states which might have developed due to change in spin exchange coupling between the cations [231,232]. It is also known that WWH loop arises from presence of different domain states, coercive fields and chemical disorder [233-236]. Basically, chemical disorder in a system induces magnetic frustration which is originated due to competitions between antiferromagnetic and ferromagnetic interactions.

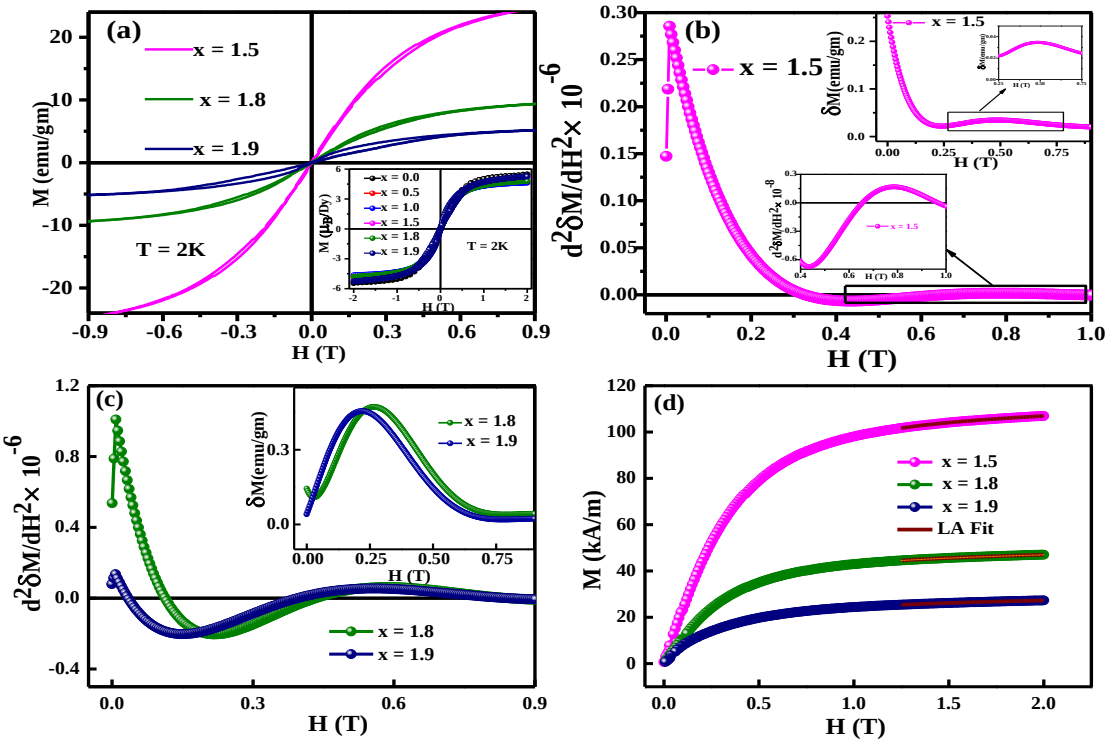

Figure 4.4(a): Zoom part of M-H curve for x = 1.5, 1.8, 1.9 samples at 2 K. **Inset**: M-H curves at 2 K for all DETO samples. **(b):** Variation of $d^2\delta M/dH^2$ curve with applied H at 2 K for x = 1.5 sample. {**Zoom part of 4.4(b)}** - $d^2\delta M/dH^2$ curve with applied H (0.4-1.0 T) at 2 K for x = 1.5 sample. **Inset**: δM between ascending and descending portions of M-H curve for x = 1.5 sample. {**Zoom part of inset 4.4(b)}-** δM of M-H curve for x = 1.5 sample from 0.25-0.75 T. **(c):** Variation of $d^2\delta M/dH^2$ curve with applied H at 2 K for x = 1.8, 1.9 samples. **Inset:** δM between ascending and descending portions of M-H curves for x = 1.8,

1.9 samples. **(d):** Descending first quadrant M-H curve for x = 1.5, 1.8, 1.9 samples with LA fit above 1 T.

Moreover, in formation of WWH loop major roles are played by the dipolar interaction (D_{nn}) and magneto-crystalline anisotropy (K_1) [237]. As has been mentioned above, the D_{nn} values were determined by fitting M(T) data with the eq (4.1). It is interesting to note that the obtained D_{nn} values are non-zero for x=1.5, 1.8, 1.9 signifying a persistent dipolar interaction which is consistent with the existence of WWH loop. It is worthwhile to mention that WWH could be found as an effect of coexistence of multi-domains and single-domains. But the samples under present investigation are bulk and therefore possibility of the existence of single domain can be discarded. Furthermore, if this was the origin then squareness should be there in the M(H) loop as observed in the case of $CoFe_2O_4$ nano powder [237]. Therefore, the possibility of single domain formation can be neglected as squareness was not found in any of the M(H) loops. Further, to find out various components causing WWH loop for x = 1.5, 1.8, 1.9, the difference between magnetization values (δM) with increasing and decreasing magnetic field were plotted against H, particularly, for first quadrant of M-H curves (shown in inset of figure 4.4b and figure 4.4c). In inset of figure 4.4b, δM curve show two anomalies (change in slope) near around 0.2 T and 0.68 T magnetic field for x = 1.5 sample. Whereas, for x = 1.8, 1.9, δM curves show two anomalies near around 0.01 T and 0.6 T magnetic field as shown in inset of figure 4.4c. The double derivative of δM curves ($d^2\delta M/dH^2$) were also plotted with H for x = 1.5, 1.8, 1.9 samples to reveal the role of different coercivities as shown in figure 4.4b and figure 4.4c. Shown in figure 4.4b, the $d^2\delta M/dH^2$ curve of x = 1.5 material instead of showing usual single peak exhibits two peaks centered on around 0.0065 T and 0.69T respectively. Two similar peaks can be seen in $d^2\delta M/dH^2$ curves of x = 1.8, 1.9 samples around 0.0055 T and 0.55 T respectively as shown in figure 4.4c. The existence of

two peaks indicates presence of two switching field distributions, resulting from the dipolar field interaction and easy plane anisotropy [237]. Similar analysis has been performed to know the origin of WWH loop for 1D $Nd_{0.1}Bi_{0.9}FeO_3$ (NBFO) nano-tubes [238] and for $CoFe_2O_4$ nano-powder [237]. In NBFO, two peaks (around 0.03 T and 1.7 T) have been observed in δM/dH curve. Low field peak is associated to low coercivity (soft component), where as high field peak is attributed to hard component [238].

Furthermore, we have also calculated the value of anisotropy constant (K_1) for x = 1.5, 1.8, 1.9. We have used the law of approach to saturation model [239] and fitted the data with the equation;

$$M = M_s\left[1-\frac{8}{105}\frac{K_1^2}{\mu_o^2 M_s^2}\frac{1}{H^2}\right] + kH, \tag{4.3}$$

where M is magnetization, M_s is saturation magnetization, K_1 is first order cubic anisotropy coefficient, H is applied magnetic field, and k is the forced magnetization coefficient and constant 8/105 deals to first order cubic anisotropy of random polycrystalline samples [240]. The descending magnetization data of first quadrant of M-H curves were fitted with eq. 4.3 above 1 T applied magnetic field at 2K as shown in figure 4.4d. We have extracted the values of K_1, M_s and k for all three samples from the fit. The obtained M_s values of x = 1.5, 1.8, 1.9 samples from the fitting of experimental data by eq. 4.3 are in agreement with magnetization value measured at applied 2 T magnetic field. The extracted K_1 values are listed in Table 4.3.

S.N.	Sample	Anisotropy Constant (K_1) (J/m^3)
1.	$\mathbf{Dy_{0.5}Eu_{1.5}Ti_2O_7}$	1.132×10^5
2.	$\mathbf{Dy_{0.2}Eu_{1.8}Ti_2O_7}$	4.603×10^4
3.	$\mathbf{Dy_{0.1}Eu_{1.9}Ti_2O_7}$	2.649×10^4

Table 4.3: Extracted anisotropy constant (K_1) values of x = 1.5, 1.8, 1.9 samples.

4.3.3.2 AC magnetic Study:

In order to examine the spin freezing and to investigate time dependent magnetic properties of doped $Dy_{2-x}Eu_xTi_2O_7$ compounds, AC susceptibility measurements were performed. Figure 4.5a shows the real part of AC susceptibility $\chi'(T)$ of x = 0.0, 0.5, 1.0 and inset (i) of figure 4.5a shows the $\chi'(T)$ of x = 1.5, 1.8, 1.9 at 500 Hz frequency and zero magnetic field. Whereas, figure 4.5b shows the corresponding imaginary part of AC susceptibility at same experimental condition. For pure DTO compound (x = 0.0), two dips appeared in $\chi'(T)$ curve around 3 K (indicated by T_i) and 16 K (indicated by T_f) and corresponding two peaks in $\chi''(T)$ are also visible. The drop around 3 K (T_i) is well known spin ice freezing transition [159,217] and the second drop around 16 K (T_f) in $\chi'(T)$ curve is associated to single ion freezing of Dy^{3+} ion [218]. The low temperature T_i spin ice freezing is present in Eu doped x = 0.5, 1.0, 1.5 samples. This indicates the robustness of spin ice state in DETO, inspite of increase in antiferromagnetic interactions between spins. Similar observations were also reported in stuffed spin ice $Ho_2(Ti_{2-x}Ho_x)O_{7-x/2}$ [241] and $Dy_2(Ti_{2-x}Dy_x)O_{7-x/2}$ [242].

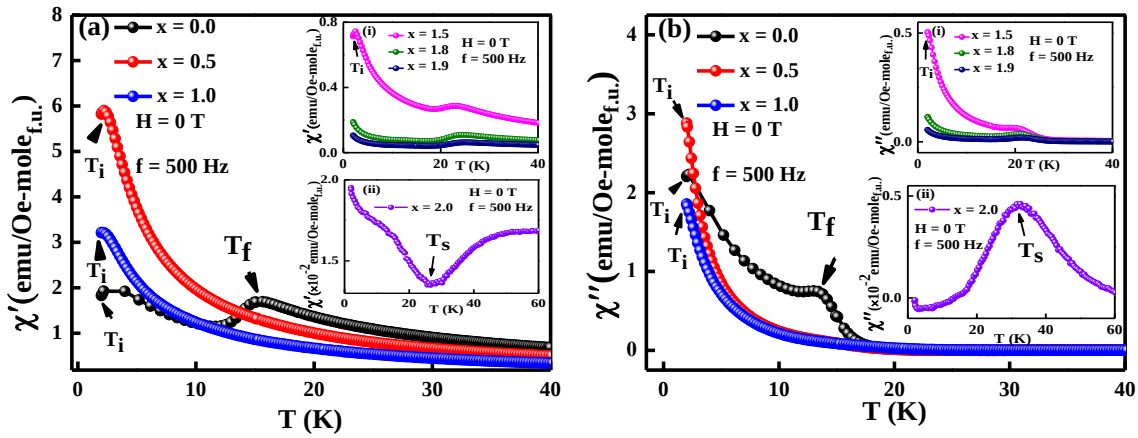

Figure 4.5(a): $\chi'(T)$ of x = 0.0, 0.5, 1.0 for f = 500 Hz at zero applied DC field. Inset **(i):** $\chi'(T)$ of x = 1.5, 1.8, 1.9 for f = 500 Hz at zero applied DC field. Inset **(ii)**: $\chi'(T)$ of x = 2.0 for f = 500 Hz at zero applied DC field. **(b):** $\chi''(T)$ of x = 0.0, 0.5, 1.0 for f = 500 Hz at zero applied DC field. Inset **(i):** $\chi''(T)$ of x = 1.5, 1.8, 1.9 for f = 500 Hz at zero applied DC field. Inset **(ii):** $\chi''(T)$ of x = 2.0 for f = 500 Hz at zero applied DC field.

In inset (i) of figure 4.5a and 4.5b, no T_i peak can be observed for x = 1.8, 1.9 samples. However, observed finite value of AC susceptibility for x = 1.8, 1.9 samples indicate that Dy^{3+} spins are still fluctuating at lower temperature (below 2 K). These low temperature outcomes are generally expected for quantum spin ice [243]. Moreover, the $\chi'(T)$ and $\chi''(T)$ curves exhibit paramagnetic behaviour at high temperature without applied magnetic field for x = 0.5, 1.0 compounds confirming the disappearance of spin freezing. Unusual nature was found for x = 1.5, 1.8, 1.9 samples, in which high temperature spin freezing has reemerged at T > 18 K [inset (i) of figure 4.5a and 4.5b]. Similar re-emergence of high temperature spin freezing was noticed for diluted spin ice $Dy_{2-x}M_xTi_2O_7$(M = Y, Lu), in which T_f peak is subdued for low levels of dilution of non – magnetic Y^{3+} and Lu^{3+} ions [218]. This T_f peak was observed to re-emerge for high dilution (x > 0.4) towards higher temperature which is dominated by single ion effect and was attributed to change in crystal field levels along with quantum mechanical and thermal processes [218]. However, the scenario is different for our $Dy_{2-x}Eu_xTi_2O_7$ systems as $Eu_2Ti_2O_7$ (x = 2.0) also shows a single ion spin freezing transition

(T_s) at 35 K which is shown in inset (ii) of figure 4.5a and 4.5b [67]. The re-entrant high temperature spin freezing for x = 1.5, 1.8, 1.9 might be associated to Eu^{3+} spins.

To find out the origin of re-entrant spin freezing in Eu rich samples, AC susceptibility was measured in presence of DC magnetic field of 2 T. An applied magnetic field let up the dynamical process and due to this there is an enhancement in χ' and χ" signals. Figure 4.6 shows the AC susceptibility [upper panel $\chi'(T)$ and lower panel $\chi''(T)$] of all doped samples at H = 2 T. For x = 0.5, 1.0, a clear transition (T_f marked by brown arrow) appeared in $\chi'(T)$ part above 16 K and a corresponding peak in $\chi''(T)$ is also observed [figure 4.6a, 4.6b]. This field dependent data is in contrast to that of H = 0 T as no high temperature peak observed is there. Furthermore, for x = 1.5 compound, an additional drop (T_s indicated by green arrow) is observed in $\chi'(T)$ around 23.5 K and corresponding peak is appeared in $\chi''(T)$ along with T_f [figure 4.6c]. Similar new additional peak (T_s) has also been observed for x = 1.8, 1.9 at higher temperature (T > 23.5 K) [figure 4.6d, 4.6e]. As a matter of fact, two peaks (T_f and T_s) are observed for x > 1.0 on applying H = 2 T magnetic field. The emergence of T_s peak in $Dy_{2-x}Eu_xTi_2O_7$ is similar to that reported in $Dy_xTb_{2-x}Ti_2O_7$, $Dy_{2-x}Gd_xTi_2O_7$ and $Dy_{2-x}Yb_xTi_2O_7$ [194, 244, 245].

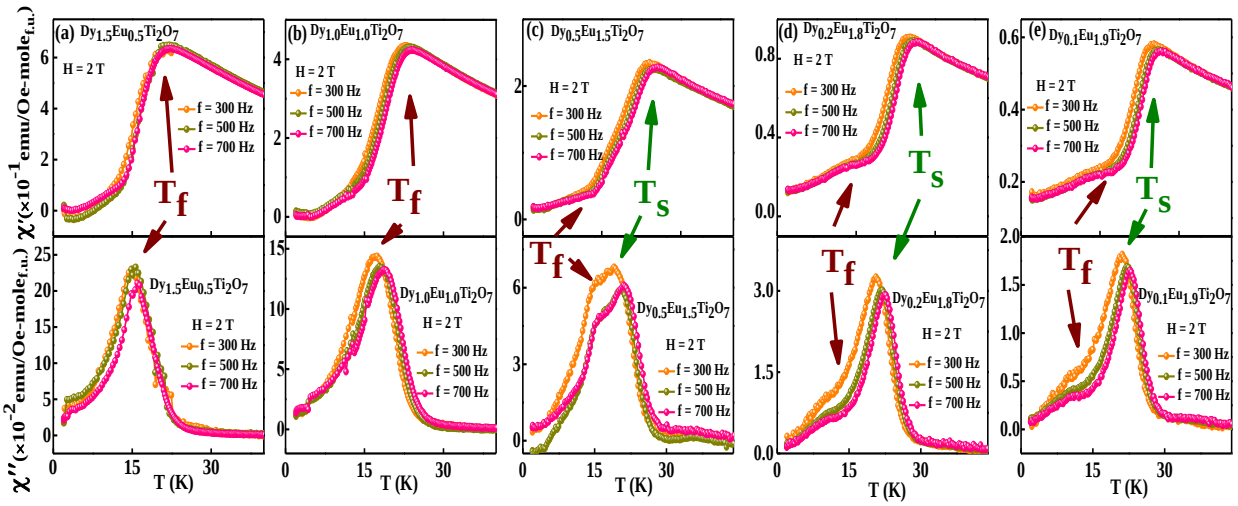

Figure 4.6: $\chi'(T)$ (upper panel) and $\chi''(T)$ (lower panel) of $Dy_{2-x}Eu_xTi_2O_7$ compounds at applied field of 2 T. **(a):** $Dy_{1.5}Eu_{0.5}Ti_2O_7$, **(b):** $Dy_{1.0}Eu_{1.0}Ti_2O_7$, **(c):** $Dy_{0.5}Eu_{1.5}Ti_2O_7$, **(d):** $Dy_{0.2}Eu_{1.8}Ti_2O_7$, **(e):** $Dy_{0.1}Eu_{1.9}Ti_2O_7$. Marked by arrow are: Single ion spin freezing peak of Dy^{3+} ions (T_f) and Single ion spin freezing peak of Eu^{3+} ions (T_s).

Both T_f and T_s transitions are thermally activated. Therefore, to confirm the nature of transition, we have fitted the frequency dependence of T_f and T_s peaks for all doped samples with Arrhenius Law,

$$f = f_0 \exp(E_a/k_bT) \qquad (4.4)$$

where, E_a is the activation energy for spin fluctuation, f_0 is a measure of the microscopic limiting frequency in the system and k_B is the Boltzmann constant. Figure 4.7a shows the Arrhenius fit. As the extracted thermal energy values of doped DETO which are linked to crystal field splitting levels, are qualitatively similar to DTO, the T_f peak can be identified as the single-ion freezing of Dy^{3+} spins. The calculated values of f_0 for T_f peak vary from 0.05 to 1.06 GHz. The extracted values of E_a for T_f and T_s peaks are shown in figure 4.7b. The variation of T_f and T_s peaks with x value in $Dy_{2-x}Eu_xTi_2O_7$ is shown in figure 4.7c. From the figures it can be seen that the T_s peak has emerged only for those samples which contain large quantity of Eu^{3+} ions ($1.5 \leq x \leq 2.0$). Derived E_a value from Arrhenius fit of T_s peak

(originated from Eu^{3+}) is increased from 277.8 K (x = 1.5) to 327.08 K (x = 1.9), whereas for pure ETO, E_a was reported to 339 K [42] and f_0 value ranges from 0.05 to 0.5 GHz. The obtained E_a value from the fitting of T_s peak is close to value assigned for single ion freezing due to Eu^{3+} spins which confirms that T_s peak is originated because of single ion freezing of Eu^{3+} ions. It is worthwhile to mention that in a recent paper it has been shown from X-ray absorption spectroscopy that Eu remains in 3+ state in ETO pyrochlore [246]. The variation in crystal field levels is due to Dy- Eu interactions, causes the systematic alteration in E_a value of T_f peak for $1.5 \leq x < 2.0$ samples. It can be further verified from the fact that crystal field effect is closely related to structural parameters like lattice constant and atomic position of oxygen atom surrounding the rare earth (A) ion [38]. From structure study, it has been found that on increasing the concentration of Eu^{3+} ions, lattice constant of DETO system increased which indicates that doping of Eu^{3+} content alters the crystal field levels. However, it is expected that activation energy value (E_a) should decrease on increasing the lattice constant. But, in contrast enhancement in E_a value was observed for present case. This nature specifies the influence of antisite disorder which causes the change in crystal-field and consequently change in energy barriers [247].

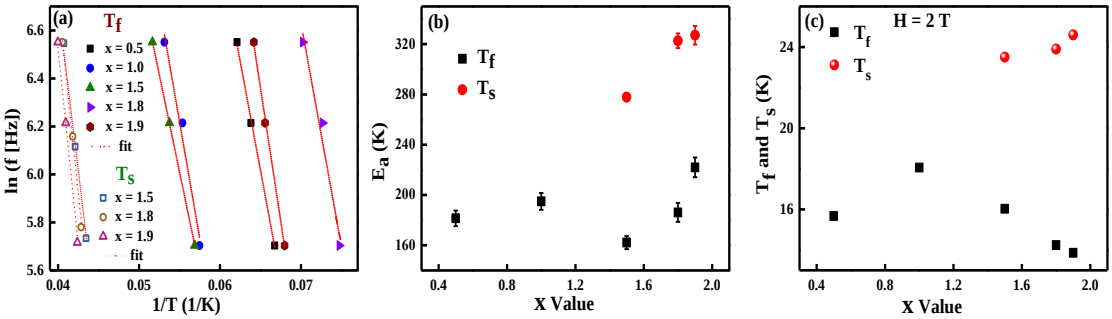

Figure 4.7(a): The Arrhenius Fit of (T_f) peak for (x = 0.5, 1.0, 1.5, 1.8, 1.9) compounds and Arrhenius Fit of (T_s) peak for (x = 1.5, 1.8, 1.9) compounds.**(b):** Variation of derived E_a values of T_f and T_s peaks with x value of $Dy_{2-x}Eu_xTi_2O_7$.**(c):** Variation of T_f and T_s peaks with x value of $Dy_{2-x}Eu_xTi_2O_7$.

From figure 4.7c, it has been observed that position of T_f peak (associated to Dy^{3+} spins) is deviated from that of x = 1.5 sample, where T_s peak (associated to Eu^{3+} spins) in introduced in DETO samples. In DETO pyrochlore (corner sharing tetrahedron structure), it is assumed that Dy^{3+} spins and Eu^{3+} spins randomly occupy the lattice of tetrahedron i.e. uniformly. So, there is hefty change in local environment of present system for particular two critical values of x(Eu) i.e. tetrahedron either consists Eu^{3+} or Dy^{3+} spins. For $x \geq 1.5$, only tetrahedron of Eu^{3+} spins appears, whereas for $x < 1.5$, only tetrahedron of Dy^{3+} spins emerges [194]. However, Dy^{3+}(Eu^{3+}) still lies in the neighborhood coordinated with six Eu^{3+}(Dy^{3+}) spins. Consequently, T_f peak is deviated from x = 1.5. This argument further suggested that T_s transition is associated to spin freezing of Eu^{3+} ions.

Furthermore, from the above discussion it is clear that x =1.5, 1.8 and 1.9 samples exhibit WWH loop and spin frustration. Therefore, existence of dipolar field, anisotropy exchange interaction and spin frustration is the origin of WWH loop in the present case.

Our observations including the compositions, frequency and magnetic field dependence of T_f and T_s peaks indicate that doping of Eu^{3+} ions at A site in DTO result the alteration in crystal-field levels. The Eu-Dy spins interaction changes this crystal field effect. Unlike other hybrid pyrochlore compounds, $Dy_{2-x}Eu_xTi_2O_7$ may be considered as combination of DTO (spin ice) and ETO. However, It is known fact that when the ferromagnetic (FM) dipolar interactions dominate over the antiferromagnetic (AFM) exchange interactions, the ground state of system is the spin ice state (two in-two out arrangement of spins). Whereas, when the AFM exchange interactions dominate over FM dipolar interactions, an all in-all out (AIAO) antiferromagnetic order can be achieved [62, 63]. The AIAO antiferromagnetic type ground state may be possible for Eu rich DETO samples. However, further muon spin relaxation

(μSR) or neutron diffraction study can describe their ground state. More experiments like specific heat measurement, neutron diffraction etc. and theoretical analysis are further needed for a clear understanding of relaxation mechanism of the present system.

4.4 Conclusion:

The Raman effect and magnetization study were carried out on $Dy_{2-x}Eu_xTi_2O_7$ pyrochlore. From the Raman effect study, it is clear that Dy is replaced by Eu. M(T) data of low Eu content samples can be fitted with the Curie-Weiss law and rich Eu containing samples can be fitted with the high temperature series expansion equation. Large Eu induces the dipolar field and anisotropy exchange interaction. The coexistence of these dipolar field and anisotropy exchange interaction induce wasp-waisted hysteresis loop in $Dy_{2-x}Eu_xTi_2O_7$ system. AC susceptibility measurement indicates the existence of both single ion spin freezing (due to Dy^{3+} and Eu^{3+} ions) in Eu rich samples. It is also observed that crystal field effect is closely related to structural parameters like lattice constant and atomic position of oxygen atom surrounding the rare earth (A) ion.